


Fast-slow analysis of a stochastic mechanism for electrical bursting


Cite as: Chaos **31**, 103128 (2021); <https://doi.org/10.1063/5.0059338>

Submitted: 08 June 2021 • Accepted: 03 September 2021 • Published Online: 26 October 2021

 Mehran Fazli, Theodore Vo and  Richard Bertram

COLLECTIONS

 This paper was selected as Featured

 This paper was selected as Scilight



[View Online](#)



[Export Citation](#)



[CrossMark](#)

Celebrate **Open Access Week** With



[LEARN MORE](#)

Fast-slow analysis of a stochastic mechanism for electrical bursting



Cite as: Chaos 31, 103128 (2021); doi: 10.1063/5.0059338

Submitted: 8 June 2021 · Accepted: 3 September 2021 ·

Published Online: 26 October 2021



View Online



Export Citation



CrossMark

Mehran Fazli,¹ Theodore Vo,² and Richard Bertram^{1,3,a}

AFFILIATIONS

¹Department of Mathematics, Florida State University, Tallahassee, Florida 32306, USA

²School of Mathematics, Monash University, Clayton, Victoria 3800, Australia

³Programs in Neuroscience and Molecular Biophysics, Florida State University, Tallahassee, Florida 32306, USA

^aAuthor to whom correspondence should be addressed: rbertram@fsu.edu. URL: <https://www.math.fsu.edu/~bertram/>

ABSTRACT

Electrical bursting oscillations in neurons and endocrine cells are activity patterns that facilitate the secretion of neurotransmitters and hormones and have been the focus of study for several decades. Mathematical modeling has been an extremely useful tool in this effort, and the use of fast-slow analysis has made it possible to understand bursting from a dynamic perspective and to make testable predictions about changes in system parameters or the cellular environment. It is typically the case that the electrical impulses that occur during the active phase of a burst are due to stable limit cycles in the fast subsystem of equations or, in the case of so-called “pseudo-plateau bursting,” canards that are induced by a folded node singularity. In this article, we show an entirely different mechanism for bursting that relies on stochastic opening and closing of a key ion channel. We demonstrate, using fast-slow analysis, how the short-lived stochastic channel openings can yield a much longer response in which single action potentials are converted into bursts of action potentials. Without this stochastic element, the system is incapable of bursting. This mechanism can describe stochastic bursting in pituitary corticotrophs, which are small cells that exhibit a great deal of noise as well as other pituitary cells, such as lactotrophs and somatotrophs that exhibit noisy bursts of electrical activity.

Published under an exclusive license by AIP Publishing. <https://doi.org/10.1063/5.0059338>

This article demonstrates how one can understand the dynamics underlying stochastic bursting in pituitary corticotrophs. These cells secrete a stress hormone when activated to produce electrical bursting. This bursting relies on one type of ion channel that is small in number but large in conductance. As a result, the current through these channels is best described as a stochastic process. This article demonstrates the mathematical basis for the bursting pattern produced by the stochastic opening and closing of these ion channels.

I. INTRODUCTION

Bursting electrical activity occurs in many neurons and endocrine cells. This pattern of activity in which electrical impulses are clustered together and the burst active phases are separated by silent phases of quiescence, is a fundamental unit of neural information^{1,2} and, in endocrine cells, is more effective than electrical spiking at evoking the secretion of hormone.^{3,4} It has long

been recognized that bursting reflects dynamics that occur on several time scales, and mathematical models of bursting cells are often analyzed using a fast-slow analysis.⁵ In this analysis, variables are partitioned into those that vary on a fast time scale and those that vary on one or more slower time scales. The dynamics of each subsystem are then analyzed and later stitched together to approximate the full system dynamics. In most cases, the bifurcation analysis of the fast subsystem, treating slow variables as slowly varying parameters, provides an explanation for the genesis of the bursting rhythm and allows one to predict the effects of varying key parameters. This approach has been used since the pioneering work of Rinzel in the 1980s.⁶

Most endocrine cells, including those in the pituitary gland, are very small, with a diameter of $7 - 15 \mu\text{m}$.⁷⁻⁹ In these small cells, the copy number of the various types of ion channels can be low, and the effects of stochastic channel opening can be pronounced.¹⁰ This is particularly true for BK channels, which are a family of K^+ channels with high single-channel conductance,¹¹ and in which copy number is low.¹⁰ For this reason, models of electrical activity in small endocrine cells often have a stochastic component, and it

was recently shown that the primary effects of stochastic channel gating can be accounted for by using a stochastic description of BK channels while treating others as deterministic.¹⁰

The primary aim of this report is to demonstrate how a model cell that produces tonic spiking can be converted to a bursting cell with the addition of stochastic openings of a few hyperpolarizing BK ion channels. As is typical for a mathematical analysis of bursting oscillations, we use a fast-slow analysis. However, unlike most cases of bursting, the fast subsystem bifurcation structure does not explain the phenomenon. Instead, invariant manifolds of fast-subsystem equilibria are the key to the behavior. This analysis not only shows why bursting occurs, but also allows us to determine the approximate number of spikes that occur in each burst active phase and thus the duration of the burst. We use a model of pituitary corticotrophs, which are cells that release the stress hormone adrenocorticotrophic hormone (ACTH) when they are bursting. Experimental studies have shown that these cells require BK channels for bursting, since pharmacological blockage or genetic knockout converts the bursting of stimulated cells to spiking.^{8,12} We demonstrate here that few BK channels are actually needed for bursting, as long as they are co-localized with Ca²⁺ channels.

II. THE MATHEMATICAL MODEL

A. The full model

The model that we employ to study corticotroph electrical activity has a 3D deterministic component that includes the cell's membrane potential (V), an activation variable for delayed rectifier K⁺ channels (n), and the free cytosolic Ca²⁺ concentration (c). The differential equations are as follow:

$$C_m \frac{dV}{dt} = -(I_{Kdr} + I_{Kir} + I_{Ca} + I_{NS} + I_L + I_{IK} + I_{BK}), \quad (1)$$

$$\frac{dn}{dt} = \frac{n_\infty - n}{\tau_n}, \quad (2)$$

$$\frac{dc}{dt} = -f_c(\alpha I_{Ca} + k_c c), \quad (3)$$

where C_m is the membrane capacitance. There are seven ionic currents: delayed rectifier K⁺ current (I_{Kdr}), inward rectifier K⁺ current (I_{Kir}), L-type Ca²⁺ current (I_{Ca}), non-selective-cation current (I_{NS}), leak current (I_L), intermediate conductance K⁺ current (I_{IK}), and big conductance K⁺ current (I_{BK}). The time constant for the activation variable n is τ_n , the fraction of Ca²⁺ that is free is denoted by f_c , the Ca²⁺ pumping rate is k_c , and the conversion from Ca²⁺ current to concentration is α . The ionic currents are given by

$$I_{Kdr} = g_{Kdr} n (V - V_K), \quad (4)$$

$$I_{Kir} = g_{Kir} r_\infty (V)(V - V_K), \quad (5)$$

$$I_{Ca} = g_{Ca} m_\infty (V)(V - V_{Ca}), \quad (6)$$

$$I_{NS} = g_{NS} (V - V_{NS}), \quad (7)$$

$$I_L = g_L (V - V_L), \quad (8)$$

$$I_{IK} = g_{IK} i_\infty (V - V_K), \quad (9)$$

$$I_{BK} = \bar{g}_{BK} (N_{z_j}^o + N_{s_n}^o + N_{z_f}^o + N_{z_n}^o) (V - V_K), \quad (10)$$

where g_x is maximal conductance for $x \in \{Kdr, Kir, Ca, NS, L, IK\}$ and \bar{g}_{BK} is the single-channel conductance of BK channels. Also, for $x \in \{K, Ca, NS, L\}$, V_x is the Nernst potential of each current. The intermediate conductance K⁺ channel activation variable, i , unlike other channels, is gated by the cytosolic Ca²⁺. Its equilibrium function is as follows:

$$i_\infty = \frac{c^2}{c^2 + k_{ik}^2}. \quad (11)$$

The other gating variables are sensitive to voltage and are governed by equations of the following form:

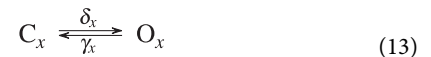
$$x_\infty = \frac{1}{1 + \exp\left(\frac{v_x - V}{s_x}\right)}, \quad (12)$$

for $x \in \{n, r, m\}$ and where v_x is the half-activation membrane voltage and s_x is the slope factor for the function. Most of the gating variables respond to changes in V and Ca²⁺ faster than do the gating variables for the delayed rectifier and BK channels and are treated as instantaneous to reduce the dimensionality and facilitate analysis.

There are two dominant types of BK channels in corticotroph cells: STREX channels and ZERO channels.¹³⁻¹⁶ The half-activation membrane potential of STREX channels is left-shifted relative to that of ZERO channels ($v_s < v_z$).^{13,16} Thus, STREX channels open at lower voltages than do ZERO channels.

The BK type of K⁺ channels are activated by both Ca²⁺ and voltage.¹⁷ BK channels that are located near Ca²⁺ channels are functionally different from those located more distant, since the "BK-near" channels are exposed to a very high Ca²⁺ concentration (over 100 μM) near the mouth of an open Ca²⁺ channel.^{18,19} In contrast, the "BK-far" channels are exposed to the bulk Ca²⁺, which has a much smaller concentration (under 0.5 μM). This means that the BK-near channels have a much higher opening rate than do the BK-far channels. Previous modeling studies have distinguished between these two types.^{12,20} We assume that some STREX and ZERO channels are colocalized with Ca²⁺ channels, while the remainder are more distant. Rather than using detailed formulations for the Ca²⁺ and voltage dependence of BK channels, we use a purely voltage-based formulation in which the channel activation rate is higher in BK-near channels, reflecting the much higher Ca²⁺ concentration to which they are exposed.

The BK channels therefore fall into four classes: ZERO-near, ZERO-far, STREX-near, and STREX-far, and the number of open BK of each class is denoted by $N_{z_n}^o$, $N_{z_f}^o$, $N_{s_n}^o$, and $N_{s_f}^o$, respectively. The state of each BK channel is then determined by a two-state Markov process,



for $x \in \{z_n, z_f, s_n, s_f\}$, and C_x and O_x represent the closed and open states, respectively. The closed-to-open transition rate is δ_x , and this

is larger for BK-near channels than for BK-far channels. The open-to-closed rate is γ_x and is the same for BK-near and BK-far channels. The opening rates are as follows:

$$\delta_{s_n} = \frac{s_\infty(V)}{\tau_{BK-n}}, \quad \delta_{z_n} = \frac{z_\infty(V)}{\tau_{BK-n}}, \quad (14)$$

$$\delta_{s_f} = \frac{s_\infty(V)}{\tau_{BK-f}}, \quad \delta_{z_f} = \frac{z_\infty(V)}{\tau_{BK-f}}, \quad (15)$$

while the closing rates are as follows:

$$\gamma_{s_n} = \frac{1 - s_\infty(V)}{\tau_{oc}}, \quad \gamma_{z_n} = \frac{1 - z_\infty(V)}{\tau_{oc}}, \quad (16)$$

$$\gamma_{s_f} = \frac{1 - s_\infty(V)}{\tau_{oc}}, \quad \gamma_{z_f} = \frac{1 - z_\infty(V)}{\tau_{oc}}. \quad (17)$$

At each time point, the state of each BK channel is updated using a uniform random number generator to choose a pseudo-random number $r \in [0, 1]$. If a channel of type x is closed at time t , then it is moved to an open state at time $t + \Delta t$ if $r < \delta_x \Delta t$; otherwise it remains closed. If the channel is open at time t , then it is moved to a closed state at time $t + \Delta t$ if $r < \gamma_x \Delta t$; otherwise, it remains open. This is done for each unblocked BK channel.

We assume that the numbers of ZERO and STREX channels are constant and denoted as N_z and N_s , respectively. This is a reasonable assumption given the short duration (5 s or less) of simulations. If β_z and β_s denote the fraction of ZERO and STREX channels colocalized with Ca^{2+} channels, then

$$N_{z_n} = \beta_z N_z \quad \text{and} \quad N_{z_f} = (1 - \beta_z) N_z, \quad (18)$$

$$N_{s_n} = \beta_s N_s \quad \text{and} \quad N_{s_f} = (1 - \beta_s) N_s. \quad (19)$$

For simplicity, we assume that $\beta_s = 0.2$, so 20% of the STREX channels are colocalized with Ca^{2+} channels. We vary the fraction of ZERO-type channels that are colocalized from 20% to 80%.

The drug paxilline is an effective and specific blocker of BK channels. When bound to a channel, paxilline puts it into a blocked state. However, even at high concentrations of paxilline not all BK channels are blocked.²¹ In our simulations, we assume that when paxilline is present, all but three BK channels are blocked at each point in time. The identity and location of the blocked channels are selected randomly at each time step. Because paxilline binds preferentially to closed channels,²² our random selection of blocked channels was biased so that closed channels are 10 times more likely to be targeted than open BK channels.

All parameter values are given in Table I, and with these values, the model produces a bursting activity pattern corresponding to a corticotroph that is stimulated with the primary hypothalamic stimulator, corticotrophin-releasing hormone (CRH). Computer simulations were performed using the Euler method in MATLAB with time step $\Delta t = 0.05$ ms. Computer code can be downloaded from www.math.fsu.edu/~bertram/software/bursting. Bifurcation diagrams were obtained using the numerical continuation software AUTO-07P.²³

TABLE I. Model parameter values for a corticotroph stimulated by CRH. Most values are from Duncan *et al.*¹² The number of BK channels is based on Richards *et al.*¹⁰

Param.	Value	Param.	Value
C_m	7 pF	v_n	-5 mV
g_{Kdr}	6.5 nS	v_m	-20 mV
g_{Kir}	0.93 nS	v_{Kir}	-50 mV
g_{Ca}	2.1 nS	v_z	-5 mV
g_{NS}	0.12 nS	v_s	-20 mV
g_L	0.2 nS	s_n	10 mV
g_{IK}	0.5 nS	s_m	12 mV
\bar{g}_{BK}	0.2 nS	s_z	2 mV
V_{Ca}	60 mV	s_s	2 mV
V_K	-70 mV	s_{Kir}	-1 mV
V_{NS}	-20 mV	α	0.0015 $\mu M/fC$
V_L	-50 mV	f_c	0.005
τ_n	30 ms	k_c	0.12 μM
τ_{BK-n}	5 ms	N_z	20
τ_{BK-f}	1000 ms	N_s	5
τ_{oc}	5 ms	β_z	0.2-0.8
k_{ik}	0.4 μ	β_s	0.2

B. The basic model

The basic model is the full model without stochastic BK channel openings, that is, without BK current. The differential equations are as follows:

$$C_m \frac{dV}{dt} = -(I_{Kdr} + I_{Kir} + I_{Ca} + I_{NS} + I_L + I_{IK}), \quad (20)$$

$$\frac{dn}{dt} = \frac{n_\infty - n}{\tau_n}, \quad (21)$$

$$\frac{dc}{dt} = -f_c(\alpha I_{Ca} + k_c c). \quad (22)$$

C. The reduced model

The reduced model is obtained from the basic model by setting the intracellular Ca^{2+} concentration to a constant. It is thus the fast subsystem of the basic model. The planar system is then

$$C_m \frac{dV}{dt} = -(I_{Kdr} + I_{Kir} + I_{Ca} + I_{NS} + I_L + I_{IK}), \quad (23)$$

$$\frac{dn}{dt} = \frac{n_\infty - n}{\tau_n}, \quad (24)$$

with c [which enters into the IK current through Eqs. (9) and (11)] treated as a parameter.

III. RESULTS

A. Bursting requires stochastic BK channel openings

Pituitary corticotrophs typically exhibit electrical bursting when stimulated with the neurohormone corticotrophin-releasing

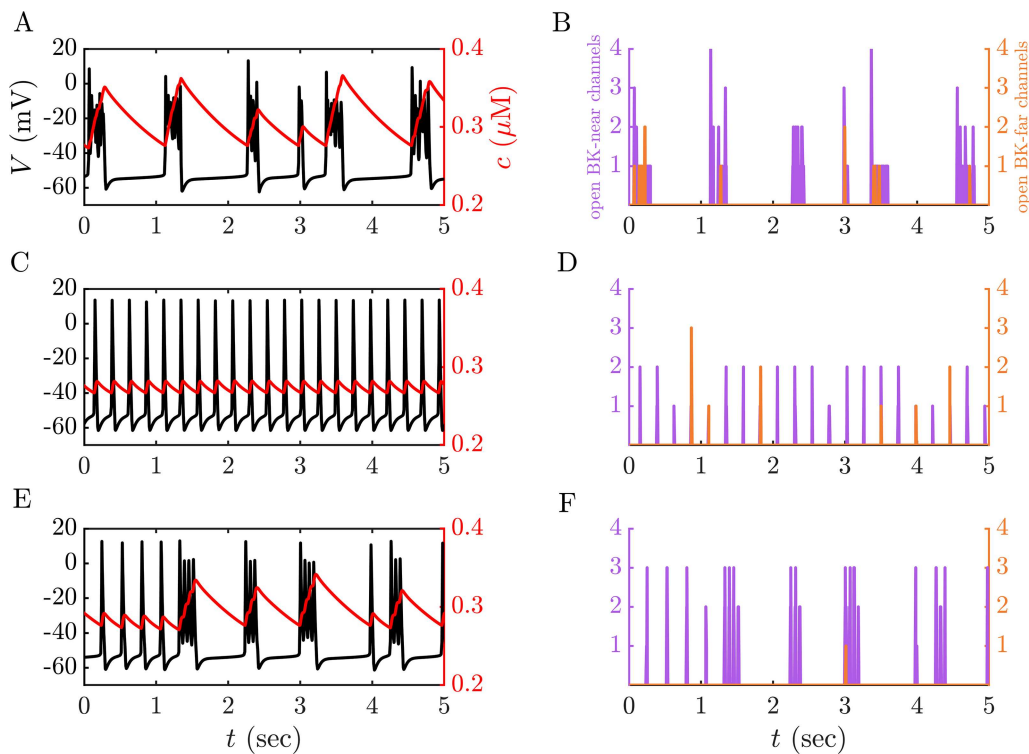


FIG. 1. Activity patterns produced by the full model, representing a corticotroph stimulated by CRH. (a) A bursting pattern is produced. The intracellular Ca^{2+} concentration is superimposed in red. (b) The number of open BK-near and BK-far channels shows episodes during bursts. (c) When the application of the BK channel antagonist paxilline is simulated by blocking 22 out of the 25 BK channels, the cell produces tonic spiking. (d) With paxilline, there are not enough BK channel openings to generate bursting. (e) Even with only 3 BK channels remaining, bursting is restored when the fraction of ZERO-type BK channels colocalized with Ca^{2+} channels is increased from $\beta_z = 0.2$ – 0.8 . (f) BK-near channel openings are now much more frequent.

hormone (CRH).⁸ This pattern of activity is replicated with the model cell, as shown in Fig. 1(a). Each burst is composed of an episode of electrical impulses or spikes, followed by a silent phase. The fast electrical spiking that occurs during a burst is in contrast to the slower changes in the superimposed intracellular Ca^{2+} concentration (c , red). The slow variation of c is the basis of fast-slow decomposition that is performed later.

During each burst, there is an episode of BK channel openings [Fig. 1(b)]. Most of these are from BK-near channels, which are colocalized with Ca^{2+} channels. The BK-type K^+ channels are necessary for bursting in corticotrophs, since the bursting is converted to tonic spiking when the BK channel antagonist paxilline is applied.⁸ This behavior is also captured by the model [Fig. 1(c)], where the effects of paxilline are simulated by putting 88% (22 channels) of the BK channels into a blocked state, while the remaining 12% (3 channels) are unblocked and can be either open or closed. This manipulation greatly reduces BK channel openings [Fig. 1(d)], and this is the reason that bursting does not occur. Bursting behavior is restored [Fig. 1(e)] by increasing the fraction of BK channels that are colocalized with Ca^{2+} channels (β_z increased from 0.2 to 0.8). The colocalized BK channels activate more quickly and with higher probability than do the others [Fig. 1(f)], which have been shown

to be important in burst production in pituitary cells.²⁴ Thus, even with only 12% of BK channels unblocked, bursting is possible if the majority of BK channels are colocalized with Ca^{2+} channels.

To explain the patterns of electrical activity shown in Fig. 1, we performed a fast-slow analysis of the basic model (i.e., the deterministic model that excludes the stochastic BK current, see Methods). An analysis of the magnitudes of the time derivatives of the three variables revealed that V and n change on a faster timescale than c (see Appendix), so in the planar reduced model (see Methods), the intracellular Ca^{2+} concentration c is treated as a parameter.

A bifurcation diagram for the reduced model with c as a bifurcation parameter is shown in Fig. 2, with full-model trajectories superimposed. The blue curves represent equilibria, while the red curves represent a branch of periodic solutions. The lower red curve gives the minimum value of V during an oscillation, while the upper one gives the maximum value. For both stationary and periodic branches, solid curves indicate stable solutions while dashed curves indicate unstable solutions.

The periodic spiking branch begins with a subcritical Hopf bifurcation and terminates with an infinite-period SNIC (Saddle-Node on Invariant Circle) bifurcation. The green curve in Fig. 2(a) is the closed orbit of the basic model and corresponds to a tonic

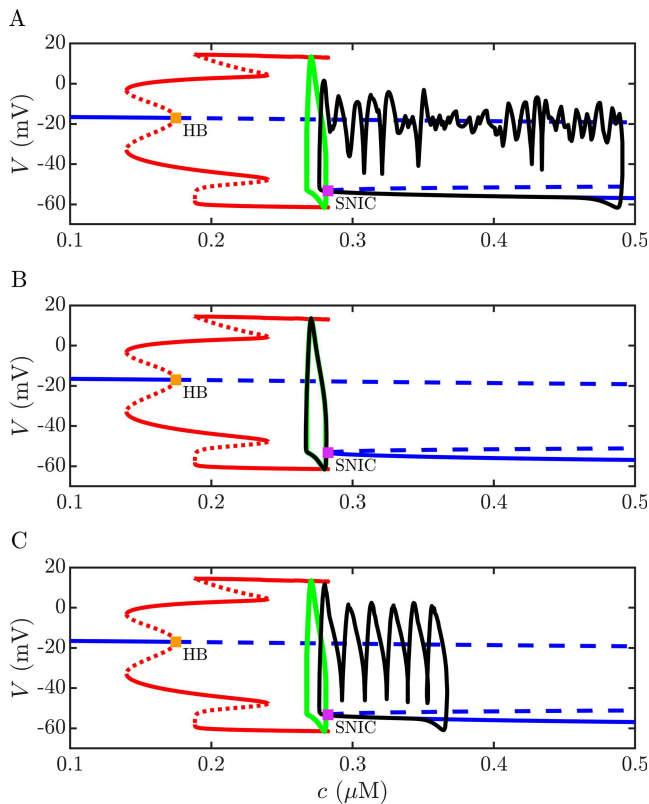


FIG. 2. Bifurcation diagrams of the reduced model, with c as a bifurcation parameter. Trajectories of the basic and full models are superimposed in green and black, respectively. Solid curves indicate stable solutions, while dashed curves indicate unstable solutions. Blue curves represent the stationary solutions, while red curves represent the periodic tonic spiking branch; the lower curve is the minimum of the oscillations, the upper curve is the maximum. HB = subcritical Hopf bifurcation at $(c, V) = (0.175, -17.00)$; SNIC = saddle-node on invariant circle bifurcation at $(c, V) = (0.283, -53.27)$. (a) Corticotroph stimulated by CRH in the full model produces bursting activity (black), cf. Fig. 1(a). (b) With simulated application of paxilline, in which 88% of the BK channels are blocked (22 of the 25 BK channels), the bursting is converted to tonic spiking [cf. Fig. 1(c)], with the orbit coincident with the spiking orbit of the basic model. (c) Increasing the fraction of ZERO-type BK channels colocalized with Ca^{2+} channels (β_2 increased from 0.2 to 0.8) restores bursting, cf. Fig. 1(e).

spiking time course. There is no bursting in the basic model, and indeed this is expected since there is no bistable interval between the stationary and periodic branches of the fast subsystem, as is required for deterministic bursting with a single slow variable.²⁵

In the full model, the closed orbit is much wider, reflecting the burst timecourse from Fig. 1(a). The genesis of bursting is not evident from the reduced model bifurcation diagram. When the application of paxilline is simulated, the burst orbit returns to a spiking orbit that is almost identical to that of the basic model [Fig. 2(b)]. Yet, when the colocalization of BK channels is increased, the bursting returns [Fig. 2(c)], though the reason is again not evident from the reduced model bifurcation diagram.

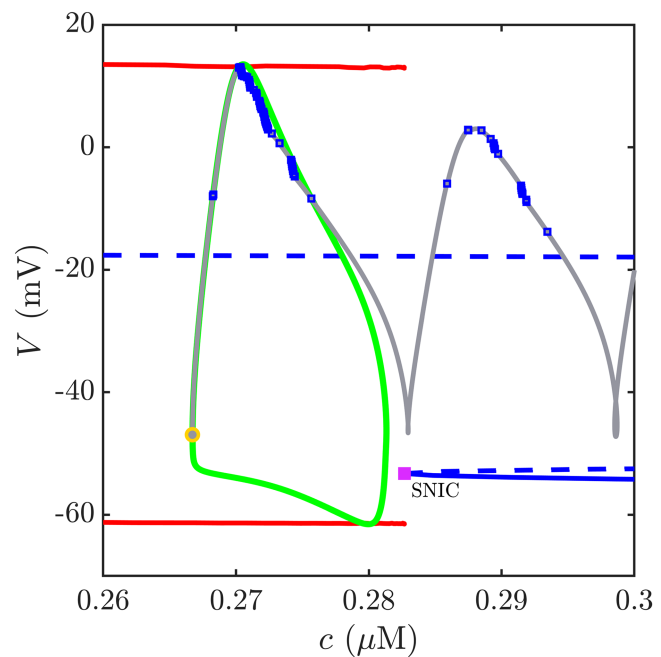


FIG. 3. Stochastic BK channel openings allow the full model system to escape the tonic spiking limit cycle of the basic model. Red and blue curves are portions of the periodic and stationary branches of the reduced model, respectively. The tonic spiking orbit is in green. The full system is started on the spiking limit cycle at the yellow circle, and its trajectory is shown in gray. BK channel openings are indicated by blue squares. These channel openings lead to a second impulse, converting spiking to bursting.

B. Escape from the spiking limit cycle mediated by stochastic BK channel openings

We now turn to the question of how the stochastic gating of BK channels can convert tonic spiking to bursting. Figure 3 is a close-up view of Fig. 2(a) with the bifurcation curves in red and blue, and the spiking limit cycle of the basic model in green. To show how the full model escapes the limit cycle to initiate a burst, it is started from a point on the spiking orbit indicated by a yellow circle and the trajectory is shown in gray. The timings of BK channel openings are shown as blue squares and do not begin until V has risen to a depolarized level of approximately -10 mV, but from this point through the remainder of the depolarized phase of the action potential they are prevalent. One effect of these channel openings is a slight decrease in the peak voltage of the impulse. A second effect occurs later, during the downstroke of the impulse, when the stochastic trajectory again deviates slightly from the spiking orbit. This deviation is important since it leads to additional spikes that make up the active phase of a burst. That is, the small deviation from the spiking orbit allows the full model system to escape and enter into a second spike rather than entering the hyperpolarized phase of the action potential. As shown in Fig. 3, the second impulse following the escape also produces a series of BK channel openings during the depolarized phase of the impulse. These channel openings are

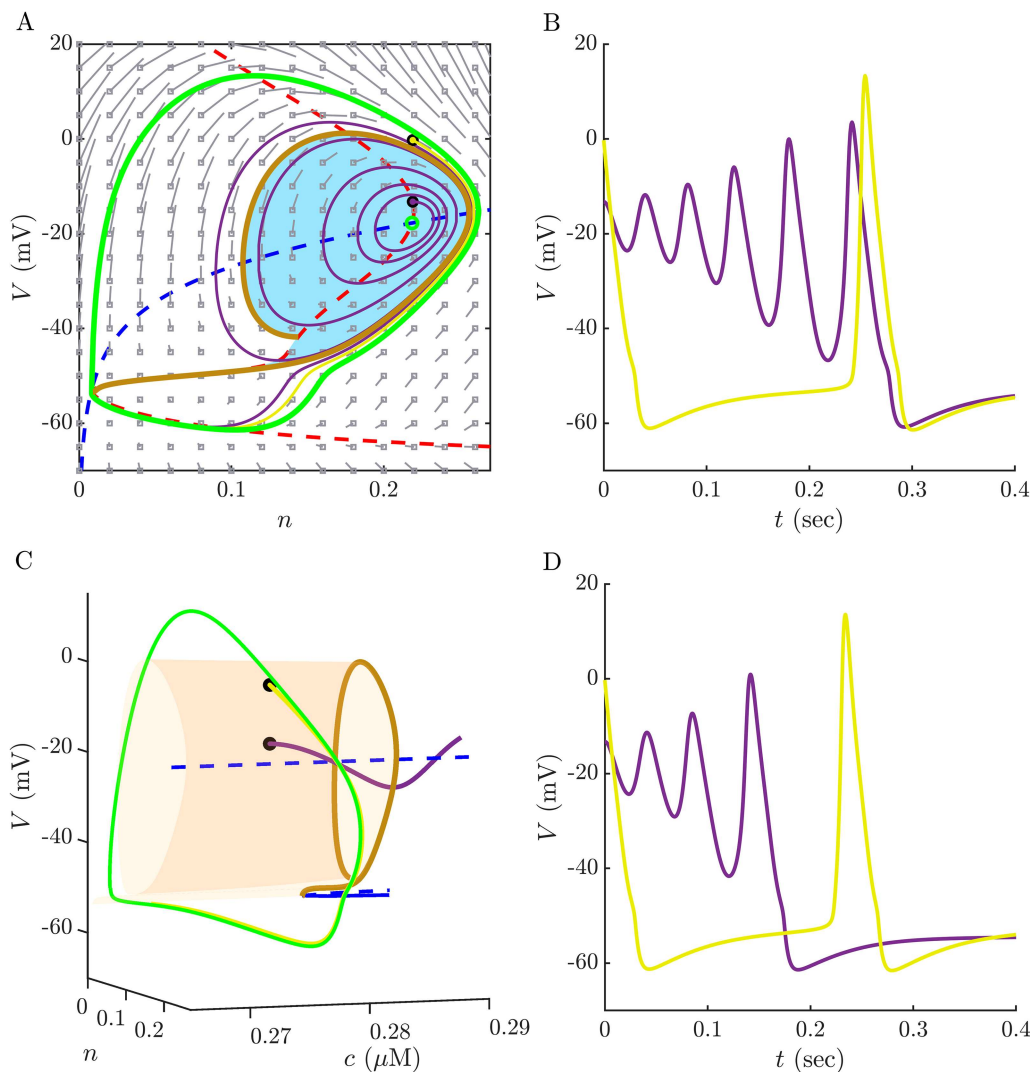


FIG. 4. Mechanism for escape from the spiking limit cycle. (a) The phase plane view of the reduced model with $c = 0.27 \mu\text{M}$, a value to the left of SNIC bifurcation. The dashed curves are nullclines (red curve is the V -nullcline, blue curve is the n -nullcline). They intersect at an unstable focus (small green circle), which is surrounded by a stable spiking limit cycle (green curve). The brown curve is a portion of the repelling slow manifold and forms a boundary for the escape region (blue shaded region). The purple orbit originates in the escape region; the yellow trajectory originates outside the escape region. (b) Burst (purple) and spiking (yellow) time courses of the reduced model corresponding to trajectories in panel (a). (c) View from the 3D phase space of the basic model. The escape boundary (brown) is extended to form a separating surface. A trajectory (purple) starting from within the separating surface moves away from the spiking limit cycle (green) as a burst is initiated. (d) Burst (purple) and spiking (yellow) time courses corresponding to trajectories of the basic model starting within and outside of, respectively, the separating surface in panel (c). Parameter values are the same as in Table I for the basic model.

sufficient to induce yet another impulse, extending the duration of the burst active phase.

C. Fast-slow analysis explains the escape phenomenon

To understand why the small deviation from the spiking orbit can produce bursting, we use the basic model and view the system in the plane of its fast subsystem, i.e., the reduced model [Fig. 4(a)],

with c fixed at a value to the left of the SNIC bifurcation, where the reduced model contains an unstable focus and a stable spiking limit cycle. The nullclines are shown as dashed curves (blue curve is the n -nullcline, red is the V -nullcline). They intersect at a single point, an unstable focus (open green circle). The spiking orbit surrounds the focus (green curve). The reduced model is itself a multiscale system, with V changing more rapidly than the recovery variable n . Thus, the spiking trajectory follows portions of the V -nullcline, as expected for a relaxation oscillation (although the time scale

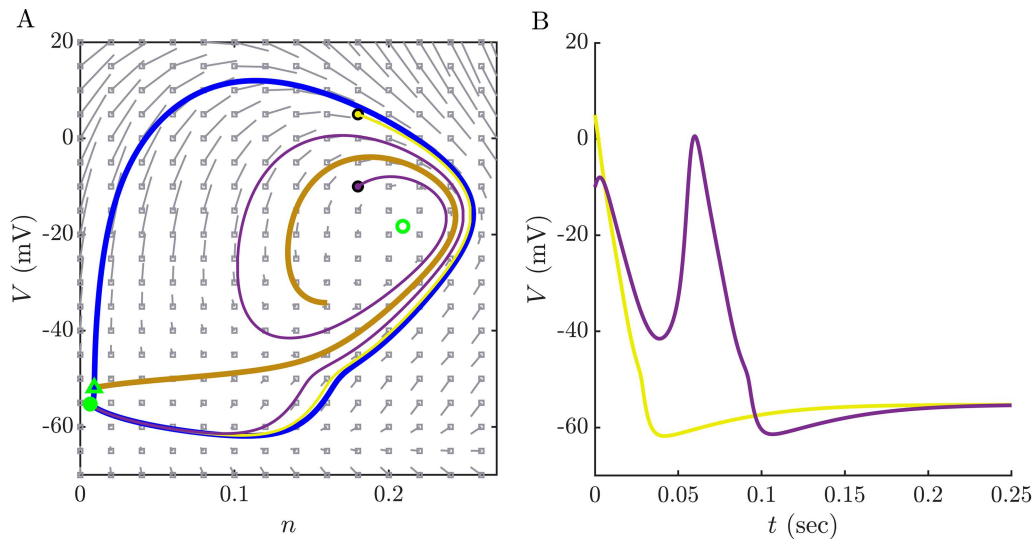


FIG. 5. Spike initiation in the fast subsystem of the basic model for $c = 0.35 \mu\text{M}$, past the SNIC bifurcation. (a) Phase plane view, showing the stable node (solid green circle), unstable focus (open green circle), and saddle point (green triangle). A portion of the repelling slow manifold of the focus, which is also a branch of the stable manifold of the saddle point, is shown in brown. The unstable manifold of the saddle point is shown in blue. Trajectories starting inside the brown curve produce an additional oscillation (purple), while those starting outside do not (yellow). (b) Time courses for the two trajectories shown in panel (a).

separation between V and n is not large enough to produce a true relaxation oscillation).

The brown curve in Fig. 4(a) is a portion of the slow repelling manifold of the focus. This curve was generated by running time backward starting at the knee of the V -nullcline. If a trajectory is initiated near the focus, then it oscillates as it moves away, with each oscillation larger than the previous one (purple trajectory). These oscillations are reflected in the slow repelling manifold; however, we show only the outermost portion of the manifold since this portion serves as a boundary. Any trajectory starting from a point in the blue shaded region of Fig. 4(a) will produce at least one small oscillation before approaching the spiking limit cycle. These small oscillations correspond to spikes in a burst active phase. The trajectory shown in purple, for example, produces a burst of five small spikes before approaching the tonic spiking limit cycle where the spikes are much larger in amplitude [Fig. 4(b)]. In contrast, a trajectory initiated outside the escape region, such as the yellow trajectory, directly approaches the spiking limit cycle without producing small spikes [Figs. 4(a) and 4(b)].

The planar analysis of Fig. 4(a) is for a fixed value of the slow variable c . The boundary curve is extended for a range of values of c in Fig. 4(c), where it is shown as a surface that we refer to as the “separating surface.” A basic model trajectory starting from within the separating surface is shown (purple curve), and a burst-like time course is shown in Fig. 4(d). During each small oscillation, the value of c increases, reflecting the opening of Ca^{2+} channels and the resultant Ca^{2+} influx, so the trajectory travels rightward through the region of phase space enclosed by the separating surface as it oscillates. In contrast, a trajectory started from outside the separating surface is immediately attracted to the spiking limit cycle [yellow curve in Figs. 4(c) and 4(d)]. The variable c increases during the

portion of the limit cycle corresponding to the more depolarized phase of an oscillation and decreases by an equal amount during the more hyperpolarized phase when fewer Ca^{2+} channels are open. Thus, we see that the separating surface separates burst trajectories, in which Ca^{2+} reaches higher levels for longer periods of time, from tonic spiking trajectories. In the full model, the opening of one or more BK channels that occurs during the falling phase of the action potential perturbs the phase point into the interior of the separating surface. As a result, the phase point escapes from the spiking limit cycle and initiates a burst.

D. Burst prolongation is achieved through re-entry into the separating surface

The explanation for burst initiation given above relies on the existence of a stable spiking limit cycle and an unstable focus in the reduced model. Soon after the start of a burst in the full model, however, the increase in c moves the system past the SNIC bifurcation (Fig. 3), and from that point until the end of the burst, the reduced model phase plane contains a stable node at a hyperpolarized voltage, a saddle point, and an unstable focus. This is illustrated in Fig. 5(a), using a value of $c = 0.35 \mu\text{M}$. Now, the repelling slow manifold of the focus connects to the saddle point, forming one branch of its stable manifold (the unstable manifold is shown as blue curves). As before, the manifold is twisted, and trajectories starting inside the region bounded by the outermost portion of the curve [shown in brown in Fig. 5(a)] exhibit small oscillations before being absorbed by the stable node. This is demonstrated with the purple trajectory, which spirals once before moving to the rest state. In the corresponding time course, this spiraling yields one extra action

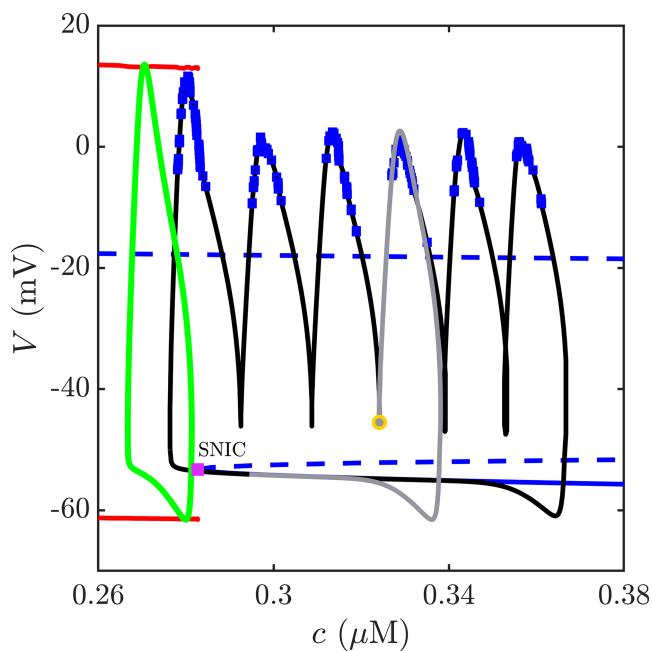


FIG. 6. Burst prolongation requires BK channel openings. A portion of the stationary (blue) and periodic (red) branches of the reduced model bifurcation diagram are shown, superimposed with the tonic spiking orbit of the basic model (green) and burst orbit of the full model (black). The timings of stochastic openings of BK channels are shown as blue squares, which occur during the depolarized phase of each spike. At the yellow circle, the BK conductance is set to 0 and the remainder of the trajectory is traced out (gray), shortening the length of the burst. Parameter values are as in Fig. 1(e).

potential [Fig. 5(b)]. In contrast, a trajectory initiated on the outside of the repelling slow manifold approaches the rest state without producing an additional action potential (yellow curves). From the analysis of the reduced model, it appears that the key to prolonging a burst so that it has more than one spike is to have the phase point perturbed to within the appropriate region of the phase plane, i.e., the region bounded by the brown curve in Fig. 5. In the full model, this is achieved by the stochastic openings of BK channels. Indeed, during the depolarized phase of each spike in a burst, there are numerous BK channel openings, and each has the potential to provide an appropriate perturbation.

The timings of BK channel openings that occur during a burst are shown superimposed on a burst orbit in Fig. 6, along with portions of the reduced system bifurcation diagram (blue and red curves) and a spiking orbit of the basic model (green curve). To demonstrate the importance of these channel openings in producing an additional spike, we performed a simulation in which the BK current conductance was set to 0 at the end of the third spike in the burst (marked by a yellow circle in Fig. 6). The remainder of that trajectory is shown as a gray curve. It completes the spike that was initiated by the BK channel openings of the previous spike, but no additional spikes are produced.

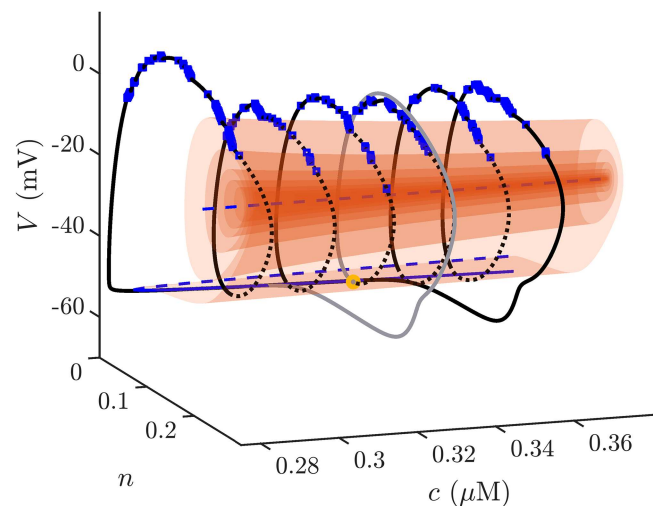


FIG. 7. The entire burst trajectory viewed from the 3D phase space. The slow repelling manifold of the unstable focus (or one branch of the stable manifold of the saddle point) is extended in the direction of c to form a twisted separating surface (red). Stochastic BK channel openings (blue squares) that occur during the depolarized phases of spikes push the full system trajectory across the surface, producing an additional spike. The gray trajectory demonstrates that if the BK conductance is set to 0 after the third spike (yellow circle), the burst terminates prematurely. Parameter values are as in Fig. 6.

The full burst is shown in the 3D phase space in Fig. 7. The slow repelling manifold from Fig. 5(a) is extended as a red surface, where the twists are evident. The BK channel openings (blue squares) occur when the burst trajectory (solid black curve) is outside of the twisted separating surface, and during the falling phase of each action potential, one of these openings pushes the trajectory across the surface (dashed portions of the trajectory are inside the surface), ensuring the production of another action potential. During the final spike, the BK channel openings fail to inject the trajectory to the interior of the surface, so no additional spike is produced and the burst active phase is terminated. The trajectory then enters a silent phase until c is sufficiently small for spiking, and the possible escape from spiking, to resume. The gray curve in the figure is the portion of the trajectory that follows from setting the BK conductance to 0 on the downstroke of the fourth spike. Removing the influence of the BK channel openings, the trajectory fails to cross into the surface, so no additional spikes are produced.

E. Burst period can be increased by injection into deep sectors of the separating surface

In the bursts shown in Fig. 7, stochastic BK channel openings repeatedly perturbed the trajectory into a separating surface sector from which an additional spike was produced. However, the burst duration can be increased further, and the spike size can be made more variable, if the stochastic channel openings perturb the trajectory into deeper sectors. This is illustrated with the basic model

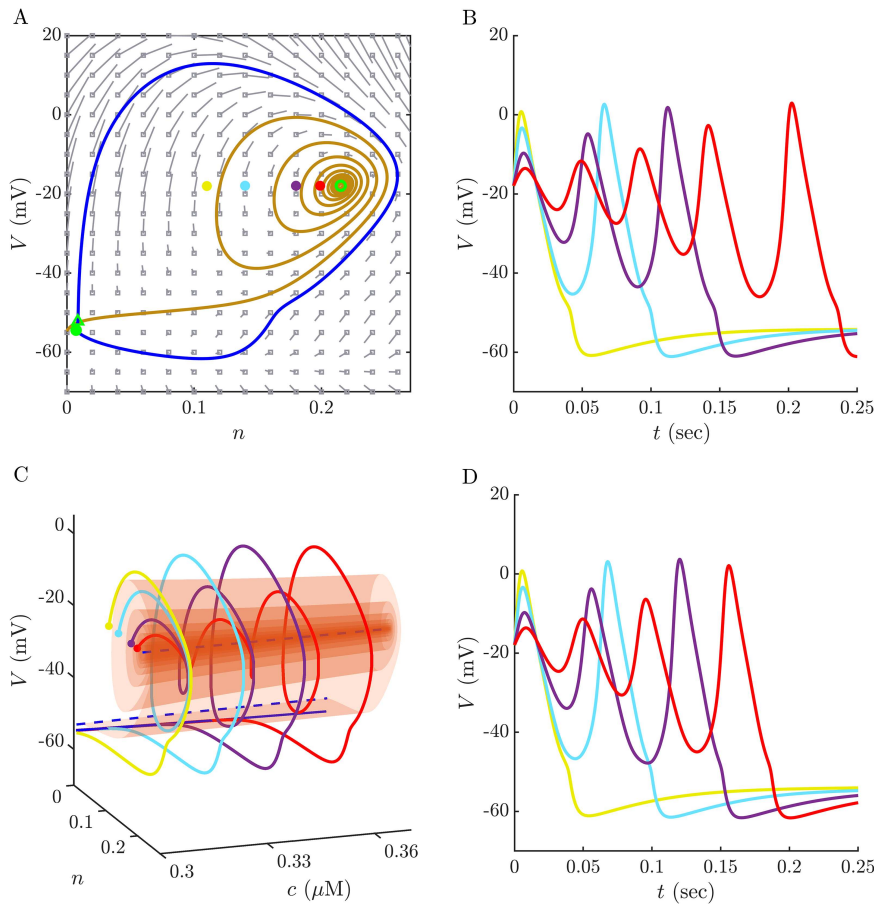


FIG. 8. Burst duration depends on the sector in which the trajectory is initiated. (a) View from the reduced model phase plane, with $c = 0.3 \mu\text{M}$. Structures are similar to those in Fig. 6, but now more of the repelling slow manifold of the focus is shown (brown curve). The four colored circles are locations in which trajectories are started. In each case, $V = -20 \text{ mV}$ and $c = 0.3 \mu\text{M}$. The n values are 0.11, 0.14, 0.18, and 0.2. (b) Time courses of the reduced model starting from different sectors of the phase plane. (c) Phase portraits of the basic model with trajectories started at the locations indicated in panel (a). (d) Time courses corresponding to the trajectories of panel (c). Parameter values are the same as in Table I for the basic model.

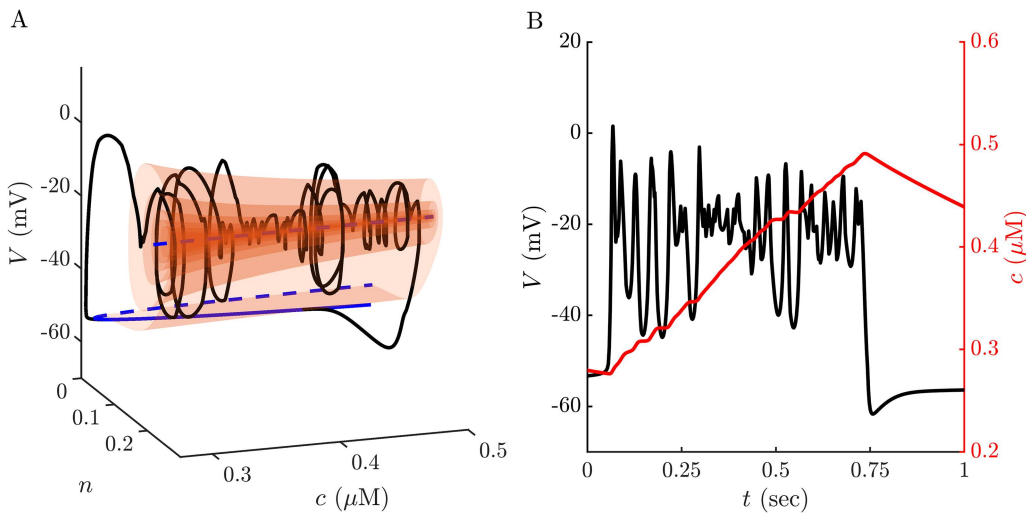


FIG. 9. A long burst produced by the full model when the trajectory enters deep sectors delimited by the separating surface. (a) The trajectory initially enters outer sectors of the separating surface, each time generating a single additional spike. Later in the burst, the trajectory is perturbed into deeper sectors, producing sequences of smaller spikes. (b) The resulting burst is unusually long and has a mix of large and small spikes. The Ca^{2+} concentration accumulates to an unusually high level during the burst. Parameter values as in Fig. 1(a).

in Fig. 8. Panel A shows initial points for four trajectories starting in different sectors of the reduced model phase plane (with $c = 0.3 \mu\text{M}$). The first point is in a sector in which a single action potential is produced as the trajectory returns to rest [yellow circle and yellow time course in panel (b)]. The second point (cyan circle) is in the first sector for additional spike production, so two spikes are produced [cyan curve in panel (b)]. The two remaining points (purple and red) are in deeper sectors, so three and five spikes are produced, respectively [purple and red curves in panel (b)].

This analysis is extended into the full 3D phase space of the basic model in Fig. 8(c). Other than the yellow trajectory, each trajectory enters the twisted separating surface at least once, resulting in the production of additional spikes in a burst. The resulting time courses shown in Fig. 8(d) are very similar to those when c was clamped [Fig. 8(b)], except that the red time course has four spikes instead of five. Although the trajectory started in a sector in which five oscillations were expected, as c increased during the burst the sectors changed and the trajectory entered a sector in which only four oscillations are produced.

Figure 9(a) is an example, shown in 3D phase space, of a very long burst produced with highly variable spike amplitudes. The first few spikes of the burst enter an outer sector, each leading to an additional spike. However, later stochastic BK channel openings inject the trajectory into deeper sectors, leading to a sequence of smaller spikes. Eventually, it fails to re-enter, and the burst terminates. The result is a time course in which the burst duration is very long, and in which the Ca^{2+} concentration rises to an unusually large value [Fig. 9(b)]. In physiological terms, a burst of activity like this would be very effective at releasing hormone.

IV. DISCUSSION

Most mathematical analyses of bursting have been applied to deterministic systems of equations.^{25–27} However, in small cells, such as most endocrine cells, stochasticity plays an important role. The more stochastic nature of the electrical activity is evident from the voltage time courses in these cells, which are noisier than what is typically observed in the larger neurons.^{10,20} As we have demonstrated in this study, stochastic channel openings can be a key ingredient to bursting in models of these cells, and their contribution can be understood using a fast-slow analysis. Unlike deterministic bursting, fast-subsystem bistability or the interaction of multiple slow variables is not required for bursting in this case. Instead, bursting was achieved through the actions of the spiral flow near a fast-subsystem unstable equilibrium.

In recent studies of model cerebellar stellate cells and fish keratocytes, it was demonstrated that the stable manifold of a saddle point can act as a threshold for spike initiation that can lead to transient oscillations in noisy systems. This was referred to as “type IV excitability.”^{28–30} This has similarities to our case when c is beyond the SNIC bifurcation and where one branch of the stable manifold of the saddle point organizes the behavior of the system. In our case, the spiral nature of the manifold provides the possibility of several spikes (Fig. 8). Also, as c varies during a burst, the fast-subsystem structure evolves from one containing limit cycle oscillations to one allowing only transient oscillations.

Our model included two isoforms of BK channels, STREX and ZERO, based on experimental evidence for both in corticotrophs.^{31–33} In this report, we did not investigate the differential roles played by these two isoforms in burst production. However, in another report we investigate this in the context of how the chronic stress affects the corticotroph electrical activity (Fazli *et al.*, submitted). The model also partitions the BK channels into populations that are close to Ca^{2+} channels and those that are far away. Although this partitioning is not based on imaging of the channel location, it is consistent with the finding in other cell types that some BK channels form complexes with Ca^{2+} -permeable channels.³⁴ Also, the effective half-activation point of BK channels at a voltage of 30 mV is greater than $10 \mu\text{M}$,³⁵ which is a level only achieved in a Ca^{2+} nanodomain that forms at the mouth of an open Ca^{2+} channel.¹⁸

Pituitary corticotrophs display several different electrical patterns when stimulated by the neurohormone CRH. These patterns include tonic spiking, plateau bursting with relatively large spikes, and pseudo-plateau bursting with very small spikes.^{8,9,12} The current study focused on plateau bursting. Models of a different pituitary cell type, the lactotroph, produce pseudo-plateau bursting in which the small spikes are induced by canards.^{27,36} It is not evident how replacing the deterministic BK current with a stochastic current would affect pseudo-plateau bursting in such models, particularly since the existence of canards is influenced by this current.³⁷ It is possible that the folded node singularity that gives rise to the canards persists, and the primary effect of the stochastic BK channel openings is to perturb the trajectory into the funnel, which would ensure the generation of one or more small spikes during a burst active phase. This question, and the general effects of stochasticity on canard-induced bursting, is a topic requiring further investigation. Pituitary cells are typically studied *in vitro* as dispersed cells. Indeed, the vast majority of electrical recordings and Ca^{2+} time courses are obtained from dispersed cells. However, *in situ*, the cells form networks in which cells of the same type are electrically coupled through gap junctions.^{38,39} This coupling effectively increases the area of the cellular membrane, which decreases the effects of stochastic channel openings.⁴⁰ The effects of electrical coupling on the stochastic bursting described herein would depend on the extent of coupling and the overall network structure. This is the focus of current investigation by our group.

ACKNOWLEDGMENTS

This work was partially supported by the National Science Foundation (NSF) under Grant No. DMS 1853342 to R.B. and T.V. The authors have no conflicts to disclose.

APPENDIX: TIME SCALE ANALYSIS

Time derivatives of the three variables reveal that V and n vary most rapidly (Fig. 10). The c variable has derivative two orders of magnitude smaller than n . This difference in time scale motivates the separation of the model equations into a fast subsystem containing V and n and a slow subsystem containing c . This separation is sufficient for understanding the dynamics of the full system, in spite of the difference in time scales of V and n variables.

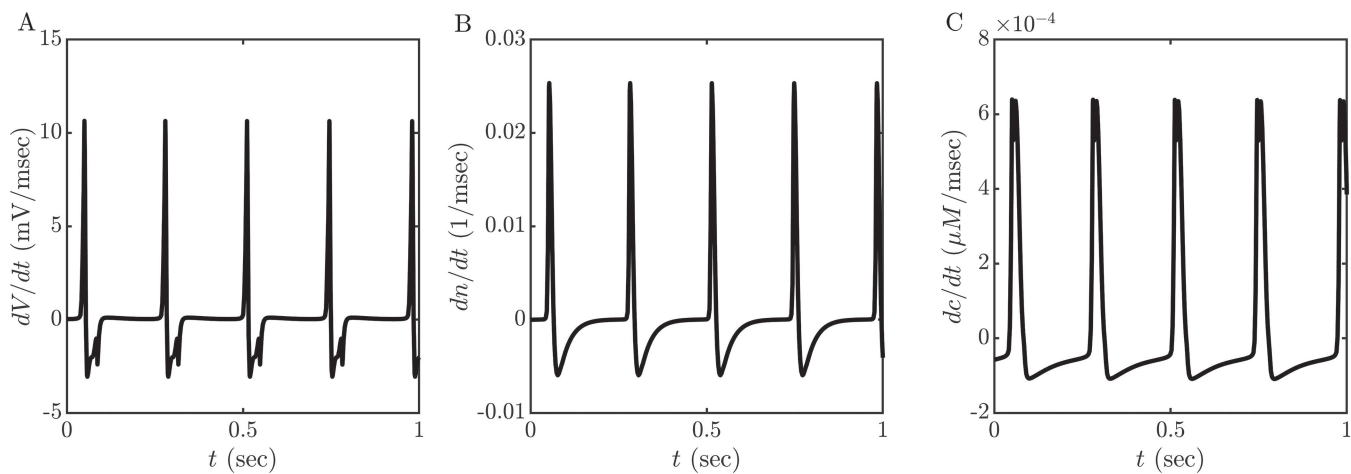


FIG. 10. Magnitudes of the time derivatives of the variables in the basic model. (a) Time derivative of V , (b) n , and (c) c .

DATA AVAILABILITY

Data sharing is not applicable to this article as no new data were created or analyzed in this study.

REFERENCES

- ¹E. M. Izhikevich, N. S. Desai, E. C. Walcott, and F. C. Hoppensteadt, "Bursts as a unit of neural information: Selective communication via resonance," *Trends Neurosci.* **26**, 161–167 (2003).
- ²J. E. Lisman, "Bursts as a unit of neural information: Making unreliable synapses reliable," *Trends Neurosci.* **20**, 38–43 (1997).
- ³A. Tagliavini, J. Tabak, R. Bertram, and M. G. Pedersen, "Is bursting more effective than spiking in evoking pituitary hormone secretion? A spatiotemporal simulation study of calcium and granule dynamics," *Am. J. Physiol.* **310**, E515–E525 (2016).
- ⁴F. Van Goor, D. Zivadinovic, A. J. Martinez-Fuentes, and S. S. Stojilkovic, "Dependence of pituitary hormone secretion on the pattern of spontaneous voltage-gated calcium influx. Cell type-specific action potential secretion coupling," *J. Biol. Chem.* **276**, 33840–33846 (2001).
- ⁵R. Bertram and J. E. Rubin, "Multi-timescale systems and fast-slow analysis," *Math. Biosci.* **287**, 105–121 (2017).
- ⁶J. Rinzel, "Bursting oscillations in an excitable membrane model," in *Ordinary and Partial Differential Equations* (Springer, Berlin, 1985), pp. 304–316.
- ⁷S. U. Kim, D. H. Shin, and G. Moretto, "Isolation, culture and cell-type identification of adult human pituitary cells," *Acta Neuropathol.* **68**, 205–208 (1985).
- ⁸P. J. Duncan, S. Sengul, J. Tabak, P. Ruth, R. Bertram, and M. J. Shipston, "Large conductance Ca^{2+} -activated K^+ channels (BK) promote secretagogue-induced transition from spiking to bursting in murine anterior pituitary corticotrophs," *J. Physiol.* **5**, 1197–1211 (2015).
- ⁹P. A. Fletcher, H. Zemkova, S. S. Stojilkovic, and A. Sherman, "Modeling the diversity of spontaneous and agonist-induced electrical activity in anterior pituitary corticotrophs," *J. Neurophysiol.* **117**, 2298–2311 (2017).
- ¹⁰D. M. Richards, J. J. Walker, and J. Tabak, "Ion channel noise shapes the electrical activity of endocrine cells," *PLoS Comput. Biol.* **16**, e1007769 (2020).
- ¹¹U. S. Lee and J. Cui, "BK channel activation: Structural and functional insights," *Trends Neurosci.* **33**, 415–423 (2010).
- ¹²P. J. Duncan, J. Tabak, P. Ruth, R. Bertram, and M. J. Shipston, "Glucocorticoids inhibit CRH/AVP-evoked bursting activity of male murine anterior pituitary corticotrophs," *Endocrinology* **157**, 3108–3121 (2016).
- ¹³L. Chen, L. Tian, S. H. MacDonald, H. McClafferty, M. S. Hammond, J. M. Huibant, P. Ruth, H. G. Knaus, and M. J. Shipston, "Functionally diverse complement of large conductance calcium- and voltage-activated potassium channel (BK) α -subunits generated from a single site of splicing," *J. Biol. Chem.* **280**, 33599–33609 (2005).
- ¹⁴G. Lai and D. P. McCobb, "Regulation of alternative splicing of Slo K^+ channels in adrenal and pituitary during the stress-hyporesponsive period of rat development," *Endocrinology* **147**, 3961–3967 (2006).
- ¹⁵M. J. Shipston, "Control of anterior pituitary cell excitability by calcium-activated potassium channels," *Mol. Cell. Endocrinol.* **463**, 37–48 (2018).
- ¹⁶L. Tian, M. S. Hammond, H. Florance, F. A. Antoni, and M. J. Shipston, "Alternative splicing determines sensitivity of murine calcium-activated potassium channels to glucocorticoids," *J. Physiol.* **537**, 57–68 (2001).
- ¹⁷H. Yang, G. Zhang, and J. Cui, "BK channels: Multiple sensors, one activation gate," *Front. Physiol.* **6**, 29 (2015).
- ¹⁸S. Simon and R. Llinás, "Compartmentalization of the submembrane calcium activity during calcium influx and its significance in transmitter release," *Biophys. J.* **48**, 485–498 (1985).
- ¹⁹A. Sherman, J. Keizer, and J. Rinzel, "Domain model for Ca^{2+} -inactivation of Ca^{2+} channels at low channel density," *Biophys. J.* **58**, 985–995 (1990).
- ²⁰K. Tsaneva-Atanasova, A. Sherman, F. Van Goor, and S. S. Stojilkovic, "Mechanism of spontaneous and receptor-controlled electrical activity in pituitary somatotrophs: Experiments and theory," *J. Neurophysiol.* **98**, 131–144 (2007).
- ²¹M. Sanchez and O. B. McManus, "Paxilline inhibition of the alpha-subunit of the high-conductance calcium-activated potassium channel," *Neuropharmacology* **35**, 963–968 (1996).
- ²²Y. Zhou and C. J. Lingle, "Paxilline inhibits BK channels by an almost exclusively closed-channel block mechanism," *J. Gen. Physiol.* **144**, 415–440 (2014).
- ²³E. J. Doedel, T. F. Fairgrieve, B. Sandstede, A. R. Champneys, Y. A. Kuznetsov, and X. Wang, see <http://indy.cs.concordia.ca/auto/> for "AUTO-07P: Continuation and Bifurcation Software for Ordinary Differential Equations" (2007).
- ²⁴J. Tabak, M. Tomaiuolo, A. E. Gonzalez-Iglesias, L. S. Milescu, and R. Bertram, "Fast-activating voltage- and calcium-dependent potassium (BK) conductance promotes bursting in pituitary cells: A dynamic clamp study," *J. Neurosci.* **31**, 16855–16863 (2011).
- ²⁵R. Bertram, M. J. Butte, T. Kiemel, and A. Sherman, "Topological and phenomenological classification of bursting oscillations," *Bull. Math. Biol.* **57**, 413–439 (1995).
- ²⁶E. M. Izhikevich, "Subcritical elliptic bursting of Bautin type," *SIAM J. Appl. Math.* **60**, 503–535 (2000).

- ²⁷T. Vo, R. Bertram, J. Tabak, and M. Wechselberger, "Mixed mode oscillations as a mechanism for pseudo-plateau bursting," *J. Comput. Neurosci.* **28**, 443–458 (2010).
- ²⁸J. Mitry, R. P. Alexander, S. Farjami, D. Bowie, and A. Khadra, "Modeling excitability in cerebellar stellate cells: Temporal changes in threshold, latency and frequency of firing," *Commun. Nonlinear Sci.* **82**, 105014 (2020).
- ²⁹S. Farjami, A. Khadra, and R. P. D. Alexander, "Switching in cerebellar stellate cell excitability in response to a pair of inhibitory/excitatory presynaptic inputs: A dynamical system perspective," *Neural Comput.* **32**, 626–658 (2020).
- ³⁰L. MacKay, E. Lehman, and A. Khadra, "Deciphering the dynamics of lamellipodium in a fish keratocytes model," *J. Theor. Biol.* **512**, 110534 (2021).
- ³¹J. Tseng-Crank, C. D. Foster, J. D. Krause, R. Mertz, N. Godinot, T. J. DiChiara, and P. H. Reinhart, "Cloning, expression, and distribution of functionally distinct Ca^{2+} -activated K^+ channel isoforms from human brain," *Neuron* **13**, 1315–1330 (1994).
- ³²J. Xie and D. P. McCobb, "Control of alternative splicing of potassium channels by stress hormones," *Science* **280**, 443–446 (1998).
- ³³M. J. Shipston, R. R. Duncan, A. G. Clark, F. A. Antoni, and L. Tian, "Molecular components of large conductance calcium-activated potassium (BK) channels in mouse pituitary corticotropes," *Mol. Endocrinol.* **13**, 1728–1737 (1999).
- ³⁴J. Zhang, X. Guan, Q. Li, A. L. Meredith, H.-L. Pan, and J. Yan, "Glutamate-activated BK channel complexes formed with NMDA receptors," *Proc. Natl. Acad. Sci. U.S.A.* **115**, E9006–E9014 (2018).
- ³⁵B. S. Rothberg and K. L. Magleby, "Gating kinetics of single large-conductance Ca^{2+} -activated K^+ channels in high Ca^{2+} suggest a two-tiered allosteric gating mechanism," *J. Gen. Physiol.* **114**, 93–124 (1999).
- ³⁶T. Vo, R. Bertram, and M. Wechselberger, "Bifurcations of canard-induced mixed mode oscillations in a pituitary lactotroph model," *Discrete Contin. Dyn. Syst.* **32**, 2879–2912 (2012).
- ³⁷T. Vo, R. Bertram, and M. Wechselberger, "Multiple geometric viewpoints of mixed mode dynamics associated with pseudo-plateau bursting," *SIAM J. Appl. Dyn. Syst.* **12**, 789–830 (2013).
- ³⁸D. J. Hodson, N. Romanò, M. Schaeffer, P. Fontanaud, C. Lafont, T. Fiordelisio, and P. Mollard, "Coordination of calcium signals by pituitary endocrine cells *in situ*," *Cell Calcium* **51**, 222–230 (2012).
- ³⁹P. R. Le Tissier, D. J. Hodson, C. Lafont, P. Fontanaud, M. Schaeffer, and P. Mollard, "Anterior pituitary cell networks," *Front. Neuroendocrinol.* **33**, 252–266 (2012).
- ⁴⁰A. Sherman, J. Rinzel, and J. Keizer, "Emergence of organized bursting in clusters of pancreatic beta-cells by channel sharing," *Biophys. J.* **54**, 411–425 (1988).